International Tables for Crystallography (2006). Vol. C, Chapter 2.5, pp. 84–88.

2.5. Energy-dispersive techniques

BY B. BURAS, W. I. F. DAVID, L. GERWARD, J. D. JORGENSEN AND B. T. M. WILLIS

2.5.1. Techniques for X-rays (By B. Buras and L. Gerward)

X-ray energy-dispersive diffraction, XED, invented in the late sixties (Giessen & Gordon, 1968; Buras, Chwaszczewska, Szarras & Szmid 1968), utilizes a primary X-ray beam of polychromatic ('white') radiation. XED is the analogue of white-beam and time-of-flight neutron diffraction (*cf.* Section 2.5.2). In the case of powdered crystals, the photon energy (or wavelength) spectrum of the X-rays scattered through a fixed optimized angle is measured using a semiconductor detector connected to a multichannel pulse-height analyser. Single-crystal methods have also been developed.

2.5.1.1. *Recording of powder diffraction spectra*

In XED powder work, the incident- and scattered-beam directions are determined by slits (Fig. 2.5.1.1). A powder spectrum is shown in Fig. 2.5.1.2. The Bragg equation is

$$2d \sin\theta_0 = \lambda = hc/E, \qquad (2.5.1.1a)$$

where d is the lattice-plane spacing, θ_0 the Bragg angle, λ and E the wavelength and the photon energy, respectively, associated with the Bragg reflection, h is Planck's constant and c the velocity of light. In practical units, equation (2.5.1.1*a*) can be written

$$E(\text{keV})\, d(\text{Å}) \sin\theta_0 = 6.199. \qquad (2.5.1.1b)$$

The main features of the XED powder method where it differs from standard angle-dispersive methods can be summarized as follows:

(*a*) The incident beam is polychromatic.

(*b*) The scattering angle $2\theta_0$ is fixed during the measurement but can be optimized for each particular experiment. There is no mechanical movement during the recording.

(*c*) The whole energy spectrum of the diffracted photons is recorded simultaneously using an energy-dispersive detector.

The scattering angle is chosen to accommodate an appropriate number of Bragg reflections within the available photon-energy range and to avoid overlapping with fluorescence lines from the sample and, when using an X-ray tube, characteristic lines from the anode. Overlap can often be avoided because a change in the scattering angle shifts the diffraction lines to new energy positions, whereas the fluorescence lines always appear at the same energies. Severe overlap problems may be encountered when the sample contains several heavy elements.

The detector aperture usually collects only a small fraction of the Debye–Scherrer cone of diffracted X-rays. The collection of an entire cone of radiation greatly increases the intensities. Also, it makes it possible to overcome crystallite stratistics problems and preferred orientations in very small samples (Holzapfel & May, 1982; Häusermann, 1992).

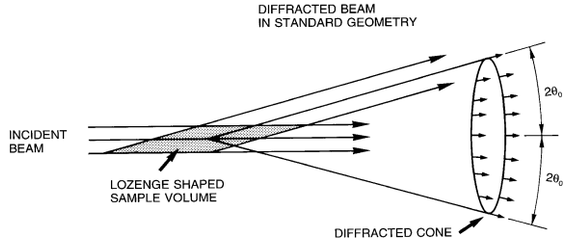

Fig. 2.5.1.1. Standard and conical diffraction geometries: $2\theta_0$ = fixed scattering angle. At low scattering angles, the lozenge-shaped sample volume is very long compared with the beam cross sections (after Häusermann, 1992).

2.5.1.2. *Incident X-ray beam*

(*a*) *Bremsstrahlung from an X-ray tube*

Bremsstrahlung from an X-ray diffraction tube provides a useful continuous spectrum for XED in the photon-energy range 2–60 keV. However, one has to avoid spectral regions close to the characteristic lines of the anode material. A tungsten anode is suitable because of its high output of white radiation having no characteristic lines in the 12–58 keV range.

A drawback of *Bremsstrahlung* is that its spectral distribution is difficult to measure or calculate with accuracy, which is necessary for a structure determination using integrated intensities [see equation (2.5.1.7)]. *Bremsstrahlung* is strongly polarized for photon energies near the high-energy limit, while the low-energy region has a weak polarization. The direction of polarization is parallel to the direction of the electron beam from the filament to the anode in the X-ray tube. Also, the polarization is difficult to measure or calculate.

(*b*) *Synchrotron radiation*

Synchrotron radiation emitted by electrons or positrons, when passing the bending magnets or insertion devices, such as wigglers, of a storage ring, provides an intense smooth spectrum for XED.

Both the spectral distribution and the polarization of the synchrotron radiation can be calculated from the parameters of the storage ring. Synchrotron radiation is almost fully polarized in the electron or positron orbit plane, *i.e.* the horizontal plane, and inherently collimated in the vertical plane. Full advantage of these features can be obtained using a vertical scattering plane. However, the mechanical construction of the diffractometer, the placing of furnaces, cryogenic equipment, *etc.* are easier to handle when the X-ray scattering is recorded in the horizontal plane. Recent XED facilities at synchrotron-radiation sources have been described by Besson & Weill (1992), Clark (1992), Häusermann (1992), Olsen (1992), and Otto (1997).

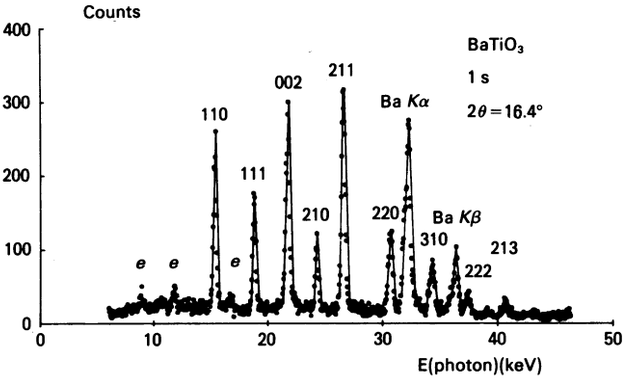

Fig. 2.5.1.2. XED powder spectrum of $BaTiO_3$ recorded with synchrotron radiation from the electron storage ring DORIS at DESY-HASYLAB in Hamburg, Germany. Counting time 1 s. Escape peaks due to the Ge detector are denoted by *e* (from Buras, Gerward, Glazer, Hidaka & Olsen, 1979).

2.5.1.3. *Resolution*

The momentum resolution in energy-dispersive diffraction is limited by the angular divergence of the incident and diffracted X-ray beams and by the energy resolution of the detector system. The observed profile is a convolution of the profile due to the angular divergence and the profile due to the detector response. For resolution calculations, it is usually assumed that the profiles are Gaussian, although the real profiles might exhibit geometrical and physical aberrations (Subsection 2.5.1.5). The relative full width at half-maximum (FWHM) of a diffraction peak in terms of energy is then given by

$$\delta E/E = [(e_n/E)^2 + 5.546F\varepsilon/E + (\cot\theta_0\Delta\theta_0)^2]^{1/2}, \quad (2.5.1.2)$$

where e_n is the electronic noise contribution, F the Fano factor, ε the energy required for creating an electron–hole pair (*cf.* Subsection 7.1.5.1), and $\Delta\theta_0$ the overall angular divergence of the X-ray beam, resulting from a convolution of the incident- and the diffracted-beam profiles. For synchrotron radiation, $\Delta\theta_0$ can usually be replaced by the divergence of the diffracted beam because of the small divergence of the incident beam.

Fig. 2.5.1.3 shows $\delta E/E$ as a function of Bragg angle θ_0. The curves have been calculated from equations (2.5.1.1) and (2.5.1.2) for two values of the lattice-plane spacing and two values of $\Delta\theta_0$, typical for *Bremsstrahlung* and synchrotron radiation, respectively. It is seen that in all cases $\delta E/E$ decreases with decreasing angle (*i.e.* increasing energy) to a certain minimum and then increases rapidly. It is also seen that the minimum point of the $\delta E/E$ curve is lower for the small d value and shifts towards smaller θ_0 values for decreasing $\Delta\theta_0$. Calculations of this kind are valuable for optimizing the Bragg angle for a given sample and other experimental conditions (*cf.* Fukamachi, Hosoya & Terasaki, 1973; Buras, Niimura & Olsen, 1978).

The relative peak width at half-height is typically less than 1% for energies above 30 keV. When the observed peaks can be fitted with Gaussian functions, one can determine the centroids of the profiles by a factor of 10–100 better than the $\delta E/E$ value of equation (2.5.1.2) would indicate. Thus, it should be possible to achieve a relative resolution of about 10^{-4} for high energies. A resolution of this order is required for example in residual-stress measurements.

The detector broadening can be eliminated using a technique where the diffraction data are obtained by means of a scanning crystal monochromator and an energy-sensitive detector (Bourdillon, Glazer, Hidaka & Bordas, 1978; Parrish & Hart, 1987). A low-resolution detector is sufficient because its function (besides recording) is just to discriminate the monochromator harmonics. The Bragg reflections are not measured simultaneously as in standard XED. The monochromator-scan method can be useful when both a fixed scattering angle (*e.g.* for samples in special environments) and a high resolution are required.

2.5.1.4. *Integrated intensity for powder sample*

The kinematical theory of diffraction and a non-absorbing crystal with a 'frozen' lattice are assumed. Corrections for thermal vibrations, absorption, extinction, *etc.* are discussed in Subsection 2.5.1.5. The total diffracted power, $P_{\mathbf{h}}$, for a Bragg reflection of a powder sample can then be written (Buras & Gerward, 1975; Kalman, 1979)

$$P_{\mathbf{h}} = hcr_e^2 VN_c^2[i_0(E)jd^2|F|^2]_{\mathbf{h}} C_p(E,\theta_0)\cos\theta_0\Delta\theta_0, \quad (2.5.1.3)$$

where $\mathbf{h}$ is the diffraction vector, r_e the classical electron radius, $i_0(E)$ the intensity per unit energy range of the incident beam evaluated at the energy of the diffraction peak, V the irradiated sample volume, N_c the number of unit cells per unit volume, j the multiplicity factor, F the structure factor, and $C_p(E,\theta_0)$ the polarization factor. The latter is given by

$$C_p(E,\theta_0) = \tfrac{1}{2}[1 + \cos^2 2\theta_0 - P(E)\sin^2 2\theta_0], \quad (2.5.1.4)$$

where $P(E)$ is the degree of polarization of the incident beam. The definition of $P(E)$ is

$$P(E) = \frac{i_{0,p}(E) - i_{0,n}(E)}{i_0(E)}, \quad (2.5.1.5)$$

where $i_{0,p}(E)$ and $i_{0,n}(E)$ are the parallel and normal components of $i_0(E)$ with respect to the plane defined by the incident- and diffracted-beam directions.

Generally, $C_p(E,\theta_0)$ has to be calculated from equations (2.5.1.4) and (2.5.1.5). However, the following special cases are sometimes of interest:

$$P = 0: \quad C_p(\theta_0) = \tfrac{1}{2}(1 + \cos^2 2\theta_0) \quad (2.5.1.6a)$$

$$P = 1: \quad C_p(\theta_0) = \cos^2 2\theta_0 \quad (2.5.1.6b)$$

$$P = -1: \quad C_p = 1. \quad (2.5.1.6c)$$

Equation (2.5.1.6*a*) can often be used in connection with *Bremsstrahlung* from an X-ray tube. The primary X-ray beam can be treated as unpolarized for all photon energies when there is an angle of 45° between the plane defined by the primary and the diffraced beams and the plane defined by the primary beam and the electron beam of the X-ray tube. In standard configurations, the corresponding angle is 0° or 90° and equation (2.5.1.6*a*) is generally not correct. However, for $2\theta_0 < 20°$ it is correct to within 2.5% for all photon energies (Olsen, Buras, Jensen, Alstrup, Gerward & Selsmark, 1978).

Equations (2.5.1.6*b*) and (2.5.1.6*c*) are generally acceptable approximations for synchrotron radiation. Equation (2.5.1.6*b*) is used when the scattering plane is horizontal and (2.5.1.6*c*) when the scattering plane is vertical.

The diffraction directions appear as generatrices of a circular cone of semi-apex angle $2\theta_0$ about the direction of incidence. Equation (2.5.1.3) represents the total power associated with this

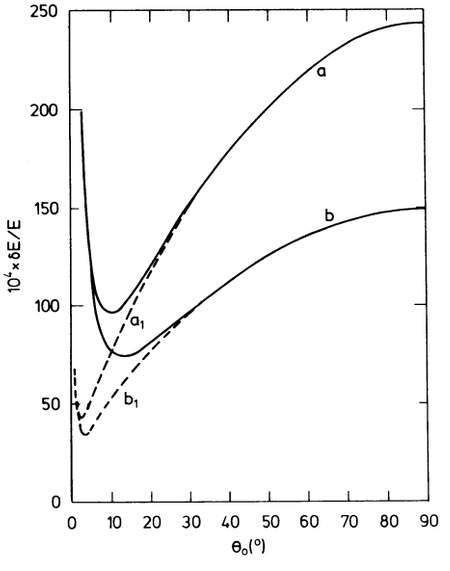

Fig. 2.5.1.3.Relative resolution, $\delta E/E$, as function of Bragg angle, θ_0, for two values of the lattice plane spacing: (*a*) 1 Å and (*b*) 0.5 Å. The full curves have been calculated for $\Delta\theta_0 = 10^{-3}$, the broken curves for $\Delta\theta_0 = 10^{-4}$.

cone. Generally, only a small fraction of this power is recorded by the detector. Thus, the useful quantity is the power per unit length of the diffraction circle on the receiving surface, $P'_{\mathbf{h}}$. At a distance r from the sample, the circumference of the diffraction circle is $2\pi r \sin 2\theta_0$ and one has (constants omitted)

$$P'_{\mathbf{h}} \propto r^{-1} V N_c^2 [i_0(E) j d^2 |F|^2]_{\mathbf{h}} \frac{C_p(E, \theta_0) \Delta\theta_0}{\sin \theta_0}. \qquad (2.5.1.7)$$

The peak areas in an XED powder spectrum are directly proportional to the $P'_{\mathbf{h}}$ of equation (2.5.1.7).

Quantitative structural analysis requires the knowledge of $i_0(E)$ and $P(E)$. As mentioned above, these quantities are not known with sufficient accuracy for *Bremsstrahlung*. For synchrotron radiation they can be calculated, but they will nevertheless contribute to the total uncertainty in the analysis. Accordingly, XED is used rather for identification of a known or assumed structure than for a full structure determination.

2.5.1.5. *Corrections*

(*a*) *Temperature effects*

The effect of thermal vibrations on the integrated intensities is expressed by the Debye–Waller factor in the same way as for standard angle-dispersive methods. Notice that $(\sin\theta)/\lambda = 1/2d$ irrespective of the method used. The contribution of the thermal diffuse scattering to the measured integrated intensities can be calculated if the elastic constants of the sample are known (Uno & Ishigaki 1975).

(*b*) *Absorption*

The transmission factor $A(E, \theta_0)$ for a small sample bathed in the incident beam and the factor $A_c(E, \theta_0)$ for a large sample intercepting the entire incident beam are the same as for monochromatic methods (Table 6.3.3.1). However, when they are applied to energy-dispersive techniques, one has to note that the absorption corrections are strongly varying with energy. In the special case of a symmetrical reflection where the incident and diffracted beams each make angles θ_0 with the face of a thick sample (powder or imperfect crystal), one has

$$A_c(E) = \frac{1}{2\mu(E)}, \qquad (2.5.1.8)$$

where $\mu(E)$ is the linear attentuation coefficient evaluated at the energy associated with the Bragg reflection.

(*c*) *Extinction and dispersion*

Extinction and dispersion corrections are applied in the same way as for angle-dispersive monochromatic methods. However, in XED, the energy dependence of the corrections has to be taken into account.

(*d*) *Geometrical aberrations*

These are distortions and displacements of the line profile by features of the geometry of the apparatus. Axial aberrations as well as equatorial divergence contribute to the angular range $\Delta\theta_0$ of the Bragg reflections. There is a predominance of positive contributions to $\Delta\theta_0$, so that the diffraction maxima are slightly displaced to the low-energy side, and show more tailing on the low-energy side than the high-energy side (Wilson, 1973).

(*e*) *Physical aberrations*

Displacements due to the energy-dependent absorption and reflectivity of the sample tend to cancel each other if the incident intensity, $i_0(E)$, can be assumed to be constant within the energy range of Bragg reflection. With synchrotron radiation, $i_0(E)$ varies rapidly with energy and its influence on the peak positions should be checked. Also, the detector response function will influence the line profile. Low-energy line shapes are particularly sensitive to the deadlayer absorption, which may cause tailing on the low-energy side of the peak. Integrated intensities, measured as peak areas in the diffraction spectrum, have to be corrected for detector efficiency and intensity losses due to escape peaks.

2.5.1.6. *The Rietveld method*

The Rietveld method (see Chapter 8.6) for refining structural variables has only recently been applied to energy-dispersive powder data. The ability to analyse diffraction patterns with overlapping Bragg peaks is particularly important for a low-resolution technique, such as XED (Glazer, Hidaka & Bordas, 1978; Buras, Gerward, Glazer, Hidaka & Olsen, 1979; Neuling & Holzapfel, 1992). In this section, it is assumed that the diffraction peaks are Gaussian in energy. It then follows from equation (2.5.1.7) that the measured profile y_i of the reflection k at energy E_i corresponding to the ith channel of the multichannel analyser can be written

$$y_i = \frac{c'}{H_k} i_0(E_i) A(E_i) j_k d_k^2 |F_k|^2 \exp\{-4 \ln 2[(E_k - E_i)^2 / H_k^2]\}, \qquad (2.5.1.9)$$

where c' is a constant, $i_0(E_i)$ is evaluated at the energy E_i, and H_k is the full width (in energy) at half-maximum of the diffraction peak. $A(E_i)$ is a factor that accounts for the absorption in the sample and elsewhere in the beam path. The number of overlapping peaks can be determined on the basis of their position and half-width. The full width at half-maximum can be expressed as a linear function of energy:

$$H_k = UE_k + V, \qquad (2.5.1.10)$$

where U and V are the half-width parameters.

2.5.1.7. *Single-crystal diffraction*

Energy-dispersive diffraction is mainly used for powdered crystals. However, it can also be applied to single-crystal diffraction.

A two-circle system for single-crystal diffraction in a diamond-anvil high-pressure cell with a polychromatic, synchrotron X-ray beam has been devised by Mao, Jephcoat, Hemley, Finger, Zha, Hazen & Cox (1988).

Formulae for single-crystal integrated intensities are well known from the classical Laue method. Adaptations to energy-dispersive work have been made by Buras, Olsen, Gerward, Selsmark & Lindegaard-Andersen (1975).

2.5.1.8. *Applications*

The unique features of energy-dispersive diffraction make it a complement to rather than a substitute for monochromatic angle-dispersive diffraction. Both techniques yield quantitative structural information, although XED is seldom used for a full structure determination. Because of the fixed geometry, energy-dispersive methods are particularly suited to *in situ* studies of samples in special environments, *e.g.* at high or low temperature and/or high pressure. The study of anomalous scattering and forbidden reflections is facilitated by the possibility of shifting the diffraction peaks on the energy scale by changing the scattering angle. Other applications are studies of Debye–Waller factors, determinative mineralogy, attenuation-coefficient measurements, on-stream measurements, particle-size and -strain

determination, and texture studies. These and other applications can be found in an annotated bibliography covering the period 1968–1978 (Laine & Lähteenmäki, 1980). The short counting time and the simultaneous recording of the diffraction spectrum permit the study of the kinetics of structural transformations in time frames of a few seconds or minutes.

Energy-dispersive powder diffraction has proved to be of great value for high-pressure structural studies in conjunction with synchrotron radiation. The brightness of the radiation source and the efficiency of the detector system permit the recording of a diffraction spectrum with satisfactory counting statistics in a reasonable time (100–1000 s) in spite of the extremely small sample volume (10^{-3}–10^{-5} mm^3). Reviews have been given by Buras & Gerward (1989) and Häusermann (1992). Recently, XED experiments have been performed at pressures above 400 GPa, and pressures near 1 TPa may be attainable in the near future (Ruoff, 1992). At this point, it should be mentioned that XED methods have limited resolution and generally give unreliable peak intensities. The situation has been transformed recently by the introduction of the image-plate area detector, which allows angle-dispersive, monochromatic methods to be used with greatly improved resolution and powder averaging (Nelmes & McMahon, 1994, and references therein).

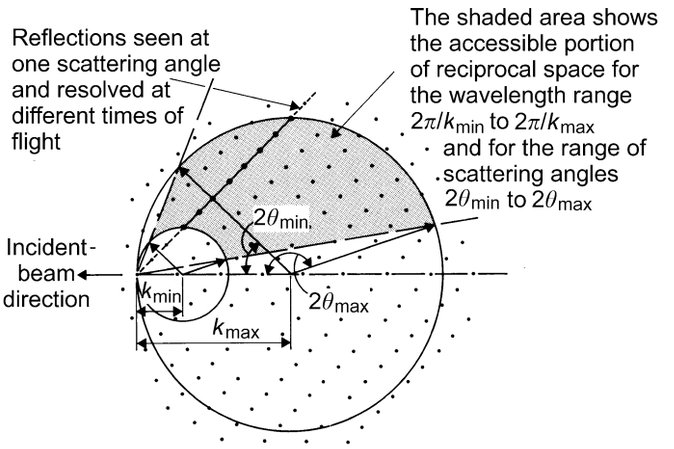

Fig. 2.5.2.1. Construction in reciprocal space to illustrate the use of multi-wavelength radiation in single-crystal diffraction. The circles with radii $k_{max} = 2\pi/\lambda_{min}$ and $k_{min} = 2\pi/\lambda_{max}$ are drawn through the origin. All reciprocal-lattice points within the shaded area may be sampled by a linear position-sensitive detector spanning the scattering angles from $2\theta_{min}$ to $2\theta_{max}$. With a position-sensitive area detector, a three-dimensional portion of reciprocal space may be examined (after Schultz, Srinivasan, Teller, Williams & Lukehart, 1984).

2.5.2. White-beam and time-of-flight neutron diffraction (By J. D. Jorgensen, W. I. F. David, and B. T. M. Willis)

2.5.2.1. *Neutron single-crystal Laue diffraction*

In traditional neutron-diffraction experiments, using a continuous source of neutrons from a nuclear reactor, a narrow wavelength band is selected from the wide spectrum of neutrons emerging from a moderator within the reactor. This monochromatization process is extremely inefficient in the utilization of the available neutron flux. If the requirement of discriminating between different orders of reflection is relaxed, then the entire white beam can be employed to contribute to the diffraction pattern and the count-rate may increase by several orders of magnitude. Further, by recording the scattered neutrons on photographic film or with a position-sensitive detector, it is possible to probe simultaneously many points in reciprocal space.

If the experiment is performed using a pulsed neutron beam, the different orders of a given reflection may be separated from one another by time-of-flight analysis. Consider a short polychromatic burst of neutrons produced within a moderator. The subsequent times-of-flight, t, of neutrons with differing wavelengths, λ, measured over a total flight path, L, may be discriminated one from another through the de Broglie relationship:

$$m_n(L/t) = h/\lambda, \qquad (2.5.2.1)$$

where m_n is the neutron mass and h is Planck's constant. Expressing t in microseconds, L in metres and λ in Å, equation (2.5.2.1) becomes

$$t = 252.7784\ L\lambda.$$

Inserting Bragg's law, $\lambda = 2(d/n)\sin\theta$, for the nth order of a fundamental reflection with spacing d in Å gives

$$t = (505.5568/n)Ld\sin\theta. \qquad (2.5.2.2)$$

Different orders may be measured simply by recording the time taken, following the release of the initial pulse from the moderator, for the neutron to travel to the sample and then to the detector.

The origins of pulsed neutron diffraction can be traced back to the work of Lowde (1956) and of Buras, Mikke, Lebech & Leciejewicz (1965). Later developments are described by Turberfield (1970) and Windsor (1981). Although a pulsed beam may be produced at a nuclear reactor using a chopper, the major developments in pulsed neutron diffraction have been associated with pulsed sources derived from particle accelerators. Spallation neutron sources, which are based on proton synchrotrons, allow optimal use of the Laue method because the pulse duration and pulse repetition rate can be matched to the experimental requirements. The neutron Laue method is particularly useful for examining crystals in special environments, where the incident and scattered radiations must penetrate heat shields or other window materials. [A good example is the study of the incommensurate structure of α-uranium at low temperature (Marmeggi & Delapalme, 1980).]

A typical time-of-flight single-crystal instrument has a large area detector. For a given setting of detector and sample, a three-dimensional region is viewed in reciprocal space, as shown in Fig. 2.5.2.1. Thus, many Bragg reflections can be measured at the same time. For an ideally imperfect crystal, with volume V_s and unit-cell volume v_c, the number of neutrons of wavelength λ reflected at Bragg angle θ by the planes with structure factor F is given by

$$N = i_0(\lambda)\lambda^4 V_s F^2/(2v_c^2\sin^2\theta), \qquad (2.5.2.3)$$

where $i_0(\lambda)$ is the number of incident neutrons per unit wavelength interval. In practice, the intensity in equation (2.5.2.3) must be corrected for wavelength-dependent factors, such as detector efficiency, sample absorption and extinction, and the contribution of thermal diffuse scattering. Jauch, Schultz & Schneider (1988) have shown that accurate structural data can be obtained using the single-crystal time-of-flight method despite the complexity of these wavelength-dependent corrections.

2.5.2.2. *Neutron time-of-flight powder diffraction*

This technique, first developed by Buras & Leciejewicz (1964), has made a unique impact in the study of powders in confined environments such as high-pressure cells (Jorgensen &

Worlton, 1985). As in single-crystal Laue diffraction, the time of flight is measured as the elapsed time from the emergence of the neutron pulse at the moderator through to its scattering by the sample and to its subsequent detection. This time is given by equation (2.5.2.2). Many Bragg peaks, each separated by time of flight, can be observed at a single fixed scattering angle, since there is a wide range of wavelengths available in the incident beam.

A good approximation to the resolution function of a time-of-flight powder diffractometer is given by the second-moment relationship

$$\Delta d/d = [(\Delta t/t)^2 + (\Delta\theta \cot\theta)^2 + (\Delta L/L)^2]^{1/2}, \qquad (2.5.2.4)$$

where Δd, Δt and $\Delta\theta$ are, respectively, the uncertainties in the d spacing, time of flight, and Bragg angle associated with a given reflection, and ΔL is the uncertainty in the total path length (Jorgensen & Rotella, 1982). Thus, the highest resolution is obtained in back scattering (large 2θ) where $\cot\theta$ is small. Time-of-flight instruments using this concept have been described by Steichele & Arnold (1975) and by Johnson & David (1985). With pulsed neutron sources a large source aperture can be viewed, as no chopper is required of the type used on reactor sources. Hence, long flight paths can be employed and this too [see equation (2.5.2.4)] leads to high resolution. For a well designed moderator the pulse width is approximately proportional to wavelength, so that the resolution is roughly constant across the whole of the diffraction pattern. For an ideal powder sample the number of neutrons diffracted into a complete Debye–Scherrer cone is proportional to

$$N' = i_0(\lambda)\lambda^4 V_s j F^2 \cos\theta \Delta\theta/(4v_c^2 \sin^2\theta) \qquad (2.5.2.5)$$

(Buras & Gerward, 1975). j is the multiplicity of the reflection and the remaining symbols in equation (2.5.2.5) are the same as those in equation (2.5.2.3).

2.4.1

Anderson, R. & Johnson, G. G. Jr (1979). *The MAX-d alphabetical index to the JCPDS data base: a new tool for electron diffraction analysis. 37th Annu. Proc. Electron Microsc. Soc. Am.*, edited by G. W. Bailey, pp. 444–445. Baton Rouge: Claitors.

Avilov, A. S., Parmon, V. S., Semiletov, S. A. & Sirota, M. I. (1984). *Intensity calculations for many-wave diffraction of fast electrons in polycrystal specimens. Kristallografiya*, **29**, 11–15. [In Russian.]

Bethe, H. A. (1928). *Theorie der Beugung von Elektronen an Kristallen. Ann. Phys. (Leipzig)*, **87**, 55–129.

Blackman, M. (1939). *On the intensities of electron diffraction rings. Proc. R. Soc. London*, **173**, 68–82.

Carr, M. J., Chambers, W. F., Melgaard, D. K., Himes, V. L., Stalick, J. K. & Mighell, A. D. (1987). *NBS/Sandia/ICDD Electron Diffraction Data Base*. Report SAND87-1992-UC-13. Sandia National Laboratories, Albuquerque, NM 87185, USA.

Cowley, J. M & Rees, A. L. G. (1947). *Refraction effects in electron diffraction. Proc. Phys. Soc.* **59**, 287–302.

Dvoryankina, G. G. & Pinsker, Z. G. (1958). *The structural study of Fe_4N. Kristallografiya*, **3**, 438–445. [In Russian.]

Goodman, P. (1963). *Investigation of arsenic trisulphide by the electron diffraction radial distribution method. Acta Cryst.* **16**, A130.

Grigson, C. W. B. (1962). *On scanning electron diffraction. J. Electron. Control,* **12**, 209–232.

Honjo, G. & Mihama, K. (1954). *Fine structure due to refraction effect in electron diffraction pattern of powder sample. J. Phys. Soc. Jpn*, **9**, 184–198.

Horstmann, M. & Meyer, G. (1962). *Messung der Elastischen Electronenbeugungsintensitaten polykristalliner Aluminium-Schichten. Acta Cryst.* **15**, 271–281.

Imamov, R. M., Pannhorst, V., Avilov, A. S. & Pinsker, Z. G. (1976). *Experimental study of dynamic effects associated with electron diffraction in partly oriented films. Kristallografiya*, **21**, 364–369.

International Tables for Crystallography (1993). Vol. B. Dordrecht: Kluwer Academic Publishers.

Mighell, A. D., Himes, V. L., Anderson, R. & Carr, M. J. (1988). *d-spacing and formula index for compound identification using electron diffraction. 46th Annu. Proc. Electron Microsc. Soc. Am.*, edited by G. W. Bailey, pp. 912–913. San Francisco Press.

Sturkey, L. & Frevel, L. K. (1945). *Refraction effects in electron diffraction. Phys. Rev.* **68**, 56–57.

Tsypursky, S. I. & Drits, V. A. (1977). *The efficiency of the electronometric measurement of intensities in electron diffraction structural studies. Izv. Akad. Nauk SSSR Ser. Phys.* **41**, 2263–2271. [In Russian.]

Turner, P. S. & Cowley, J. M. (1969). *The effect of n-beam dynamical diffraction in electron diffraction intensities from polycrystalline materials. Acta Cryst.* A**25**, 475–481.

Vainshtein, B. K. (1964). *Structure analysis by electron diffraction*. Oxford: Pergamon Press. [Translated from the Russian: *Strukturnaya Electronografiya*.]

2.4.2

Allemand, R., Bordet, J., Roudaut, E., Convert, P., Ibel, K., Jacobe, J., Cotton, J. P. & Farnoux, B. (1975). *Position sensitive detectors for neutron diffraction. Nucl. Instrum. Methods*, **126**, 29–42.

Caglioti, G., Paoletti, A. & Ricci, F. P. (1958). *Choice of collimators for a crystal spectrometer for neutron diffraction. Nucl. Instrum. Methods*, **3**, 223–228.

Carlile, C. J., Hey, P. D. & Mack, B. (1977). *High efficiency Soller slit collimators for thermal neutrons. J. Phys. E*, **10**, 543–546.

Hewat, A. W. (1975). *Design for a conventional high resolution neutron powder diffractometer. Nucl. Instrum. Methods*, **127**, 361–370.

Hewat, A. W. (1986*a*). *D2B, a new high resolution neutron powder diffractometer at ILL Grenoble. Mater. Sci. Forum*, **9**, 69–79.

Hewat, A. W. (1986*b*). *High resolution neutron and synchrotron powder diffraction. Chem. Scr.* **26**A, 119–130.

Hewat, A. W. & Bailey, I. (1976). *D1A, a high resolution neutron powder diffractometer with a bank of Mylar collimators. Nucl. Instrum. Methods*, **137**, 463–471.

Howard, C. J. (1982). *The approximation of asymmetric neutron powder diffraction peaks by sums of Gaussians. J. Appl. Cryst.* **15**, 615–620.

Loopstra, B. O. (1966). *Neutron powder diffractometry using a wavelength of 2.6 Å. Nucl. Instrum. Methods*, **44**, 181–187.

Rietveld, H. M. (1969). *A profile refinement method for nuclear and magnetic structures. J. Appl. Cryst.* **2**, 65–71.

Wilson, A. J. C. (1963). *Mathematical theory of X-ray powder diffractometry*. Eindhoven: Centrex.

2.5.1

Besson, J. M. & Weill, G. (1992). *EDX station for high pressure at LURE (DCI). High Press. Res.* **8**, 715–716.

Bourdillon, A. J., Glazer, A. M., Hidaka, M. & Bordas, J. (1978). *High-resolution energy-dispersive diffraction using synchrotron radiation. J. Appl. Cryst.* **11**, 684–687.

Buras, B., Chwaszczewska, J., Szarras, S. & Szmid, Z. (1968). *Fixed angle scattering* (*FAS*) *method for X-ray crystal structure analysis*. Report No. 894/II/PS, 10 pp. Institute of Nuclear Research, Warsaw.

Buras, B. & Gerward, L. (1975). *Relations between integrated intensities in crystal diffraction methods for X-rays and neutrons. Acta Cryst.* A**31**, 372–374.

Buras, B. & Gerward, L. (1989). *Application of X-ray energy-dispersive diffraction for characterization of materials under high pressure. Prog. Cryst. Growth Charact.* **18**, 93–138.

Buras, B., Gerward, L., Glazer, A. M., Hidaka, M. & Olsen, J. S. (1979). *Quantitative structural studies by means of the energy-dispersive method with X-rays from a storage ring. J. Appl. Cryst.* **12**, 531–536.

Buras, B., Niimura, N. & Olsen, J. S. (1978). *Optimum resolution in X-ray energy-dispersive diffractometry. J. Appl. Cryst.* **11**, 137–140.

Buras, B., Olsen, J. S., Gerward, L., Selsmark, B. & Lindegaard-Andersen, A. (1975). *Energy-dispersive spectroscopic methods applied to X-ray diffraction in single crystals. Acta Cryst.* A**31**, 327–333.

Clark, S. M. (1992). *A new white beam single crystal and powder diffraction facility at the SRS. Rev. Sci. Instrum.* **63**, 1010–1012.

Fukamachi, T., Hosoya, S. & Terasaki, O. (1973). *The precision of interplanar distances measured by an energy-dispersive method. J. Appl. Cryst.* **6**, 117–122.

2.5.1 (*cont.*)

Giessen, B. C. & Gordon, G. E. (1968). *X-ray diffraction: new high-speed technique based on X-ray spectroscopy*. *Science*, **159**, 973–975.

Glazer, A. M., Hidaka, M. & Bordas, J. (1978). *Energy-dispersive powder profile refinement using synchrotron radiation*. *J. Appl. Cryst.* **11**, 165–172.

Häusermann, D. (1992). *New techniques for new sources: a fresh look at energy-dispersive diffraction for high-pressure studies*. *High Press. Res.* **8**, 647–654.

Holzapfel, W. B. & May, W. (1982). *Improvements in energy dispersive X-ray diffraction with conical slit and diamond cell. High-pressure research in geophysics*, edited by S. Akimoto & M. H. Manghnani, pp. 73–80, and references therein. Dordrecht: Reidel.

Kalman, Z. H. (1979). *On the derivation of integrated reflected energy formulae*. *Acta Cryst.* A**35**, 634–641.

Laine, E. & Lähteenmäki, I. (1980). *The energy-dispersive X-ray diffraction method*: *annotated bibliography 1968–78*. *J. Mater. Sci.* **15**, 269–278, and references therein.

Mao, H. K., Jephcoat, A. P., Hemley, R. J., Finger, L. W., Zha, C. S., Hazen, R. M. & Cox, D. E. (1988). *Synchrotron X-ray diffraction measurements of single crystal hydrogen to 26.5 GigaPascals*. *Science*, **239**, 1131–1134.

Nelmes, R. J. & McMahon, M. I. (1994). *High-pressure powder diffraction on synchrotron sources*. *J. Synchrotron Rad.* **1**, 69–73.

Neuling, H. W. & Holzapfel, W. B. (1992). *Rietveld analysis for energy dispersive X-ray diffraction under high pressure with synchrotron radiation*. *High Press. Res.* **8**, 665–660.

Olsen, J. S. (1992). *Instrumentation for high-pressure X-ray diffraction research at HASYLAB*. *Rev. Sci. Instrum.* **63**, 1058–1061.

Olsen, J. S., Buras, B., Jensen, T., Alstrup, O., Gerward, L. & Selsmark, B. (1978). *Influence of polarization of the incident beam on integrated intensities in X-ray energy-dispersive diffractometry*. *Acta Cryst.* A**34**, 84–87.

Otto, J. W. (1997). *A facility for high-pressure X-ray diffraction at HASYLAB*. *Nucl. Instrum. Methods*, A**384**, 552–557.

Parrish, W. & Hart, M. (1987). *Advantages of synchrotron radiation for polycrystalline diffractometry*. *Z. Kristallogr.* **179**, 161–173.

Ruoff, A. L. (1992). *EDXD studies above 400 GPa (and prospects for obtaining pressures near 1 TPa and doing EDXD studies at such pressures)*. *High Press. Res.* **8**, 639–645.

Uno, R. & Ishigaki, A. (1975). *The correction of experimental structure factors for thermal diffuse scattering in white X-ray diffraction*. *Jpn. J. Appl. Phys.* **14**, 291–292.

Wilson, A. J. C. (1973). *Note on the aberrations of a fixed-angle energy-dispersive powder diffractometer*. *J. Appl. Cryst.* **6**, 230–237.

2.5.2

Buras, B. & Gerward, L. (1975). *Relations between integrated intensities in crystal diffraction methods for X-rays and neutrons*. *Acta Cryst.* A**31**, 372–374.

Buras, B. & Leciejewicz, J. (1964). *A new method for neutron diffraction crystal structure investigations*. *Phys. Status Solidi*, **4**, 349–355.

Buras, B., Mikke, K., Lebech, B. & Leciejewicz, J. (1965). *The time-of-flight method for investigations of single-crystal structures*. *Phys. Status Solidi*, **11**, 567–573.

Jauch, W., Schultz, A. J. & Schneider, J. R. (1988). *Accuracy of single crystal time-of-flight neutron diffraction: a comparative study of MnF_2*. *J. Appl. Cryst.* **21**, 975–979.

Johnson, M. W. & David, W. I. F. (1985). *HPRD: the high resolution powder diffractometer at the spallation neutron source*. Report RAL-85-112. Rutherford Appleton Laboratory, Chilton, Didcot, Oxon, UK.

Jorgensen, J. D. & Rotella, F. J. (1982). *High-resolution time-of-flight powder diffractometer at the ZING-P′ pulsed neutron source*. *J. Appl. Cryst.* **15**, 27–34.

Jorgensen, J. D. & Worlton, T. G. (1985). *Disordered structure of D_2O ice VII from in situ neutron powder diffraction*. *J. Chem. Phys.* **83**, 329–333.

Lowde, R. D. (1956). *A new rationale of structure-factor measurement in neutron-diffraction analysis*. *Acta Cryst.* **9**, 151–155.

Marmeggi, J. C. & Delapalme, A. (1980). *Neutron Laue photographs of crystallographic satellite reflections in alpha-uranium*. *Physica (Utrecht)*, **102**B, 309–312.

Schultz, A. J., Srinivasan, K., Teller, R. G., Williams, J. M. & Lukehart, C. M. (1984). *Single-crystal time-of-flight neutron diffraction structure of hydrogen cis-diacetyltetracarbonylrhenate*. *J. Am. Chem. Soc.* **106**, 999–1003.

Steichele, E. & Arnold, P. (1975). *A high-resolution neutron time-of-flight diffractometer*. *Phys. Lett.* A**44**, 165–166.

Turberfield, K. C. (1970). *Time-of-flight neutron diffractometry*. *Thermal neutron diffraction*, edited by B. T. M. Willis, pp. 34–50. Oxford University Press.

Windsor, C. G. (1981). *Pulsed neutron diffraction*. London: Taylor & Francis.

2.6.1

Anderegg, J. W., Beeman, W. W., Shulman, S. & Kaesberg, P. J. (1955). *An investigation of the size, shape and hydration of serum albumin by small-angle X-ray scattering J. Am. Chem. Soc.* **77**, 2927–2937.

Bayvel, L. P. & Jones, A. R. (1981). *Electromagnetic scattering and its applications*. London: Applied Science Publishers.

Bonse, U. & Hart, M. (1965). *An X-ray interferometer*. *Appl. Phys. Lett.* **6**, 155–156.

Bonse, U. & Hart, M. (1966). *An X-ray interferometer*. *Z. Phys.* **189**, 151–156.

Bonse, U. & Hart, M. (1967). In *Small-angle X-ray scattering,* edited by H. Brumberger. New York: Gordon and Breach.

Bracewell, R. (1986). *Fourier transform and its applications*. New York: McGraw-Hill.

Brumberger, H. (1967). *Small-angle X-ray scattering*. New York: Gordon and Breach.

Chen, S. H., Sheu, E. Y., Kalus, J. & Hoffmann, H. (1988). *Small-angle neutron scattering investigation of correlations in charged macromolecular and supramolecular solutions*. *J. Appl. Cryst.* **21**, 751–769.

Cleemann, J. C. & Kratky, O. (1960). *Größe, Gestalt und Solvatation des Edestinmoleküls aus dem Studium der Röntgenkleinwinkelstreuung*. *Z. Naturforsch. Teil B*, **15**, 525–535.

Damaschun, G., Damaschun, H., Müller, J. J., Ruckpaul, K. & Zinke, M. (1974). *Vergleich der Struktur von Proteinen im Kristall und in Lösung; Theoretische und experimentelle Untersuchungen mittels der Röntgen-Klein-winkelstreuung am Hämoglobin*. *Stud. Biophys.* **47**, 27–39.